Monthly Notices
of the
ROYAL ASTRONOMICAL SOCIETY

MNRAS **486,** 4805–4812 (2019)
Advance Access publication 2019 April 30

doi:10.1093/mnras/stz1172

Nitrogen fractionation in external galaxies

Serena Viti,[1]★ Francesco Fontani,[2] Izaskun Jiménez-Serra[1,3] and Jonathan Holdship[1]

[1]*University College London, Gower Street, London WC1E 6BT, UK*
[2]*Osservatorio Astrofisico di Arcetri, Largo E. Fermi 2, I-50125 Firenze, Italy*
[3]*Centro de Astrobiología (CSIC/INTA), Ctra de Torrejón a Ajalvir, km 4, E-28850 Torrejón de Ardoz, Madrid, Spain*

Accepted 2019 April 25. Received 2019 March 25; in original form 2018 December 12

ABSTRACT

In star-forming regions in our own Galaxy, the $^{14}N/^{15}N$ ratio is found to vary from ∼100 in meteorites, comets, and protoplanetary discs up to ∼1000 in pre-stellar and star-forming cores, while in external galaxies the very few single-dish large-scale measurements of this ratio lead to values of 100–450. The extent of the contribution of isotopic fractionation to these variations is, to date, unknown. In this paper, we present a theoretical chemical study of nitrogen fractionation in external galaxies in order to determine the physical conditions that may lead to a spread of the $^{14}N/^{15}N$ ratio from the solar value of ∼440 and hence evaluate the contribution of chemical reactions in the interstellar medium (ISM) to nitrogen fractionation. We find that the main cause of ISM enrichment of nitrogen fractionation is high gas densities, aided by high fluxes of cosmic rays.

Key words: ISM: abundances – ISM: molecules – galaxies: ISM.

1 INTRODUCTION

Nitrogen is the fifth most abundant element in the Universe that can exist in the form of two stable isotopes, ^{14}N and ^{15}N. The $^{14}N/^{15}N$ ratio has been measured in Solar system objects such as comets, meteorites, and chondrites (Mumma & Charnley 2011; Füri & Marty 2015), in molecular clouds with and without the influence of star formation processes (Adande & Ziurys 2012; Bizzocchi et al. 2013; Hily-Blant et al. 2013; Fontani et al. 2015; Guzmán et al. 2017; Zeng et al. 2017; Colzi et al. 2018a,b; De Simone et al. 2018; Kahane et al. 2018; Redaelli et al. 2018), and in galaxies (Henkel et al. 1998, 2018; Chin et al. 1999). In star-forming regions, there is a large spread in the measured $^{14}N/^{15}N$ ratio, ranging from ∼100 for meteorites, comets, and protoplanetary discs to ∼1000 in pre-stellar and star-forming cores. The solar nebula value measured in the solar wind and in Jupiter's atmosphere is an intermediate value, around 440 (Fouchet et al. 2004; Marty, Kelley & Turner 2010). In the few extragalactic sources where the $^{14}N/^{15}N$ ratio has been measured, its values range from ∼100 to 450 (see Table 1).

The $^{14}N/^{15}N$ ratio is considered a good indicator of stellar nucleosynthesis, since the two isotopes are not synthesized in the same way. Both isotopes are thought to be actively produced in the CNO cycles of massive stars and in the so-called hot bottom burning of asymptotic giant branch (AGB) stars (e.g. Schmitt & Ness 2002; Izzard et al. 2004). However, there should be some differences in their nucleosynthesis necessary to explain their observational behaviour, such as the strong primary component of ^{14}N at low metallicity (e.g. Matteucci 1986), or the relative role played by massive stars and novae in the (over)production of ^{15}N with respect to ^{14}N (e.g. Clayton 2003; Romano & Matteucci 2003; Prantzos 2011; Romano et al. 2017). The relative importance of these processes, and the existence of additional processes not yet considered, is still unclear. In particular, the contribution of the isotopic fractionation, i.e. the role of chemical reactions occurring in the gas phase of the interstellar medium (ISM; see e.g. Roueff, Loison & Hickson 2015; Wirström & Charnley 2018), which are unrelated to stellar nucleosynthesis, has not been explored in detail under the different physical conditions expected in extragalactic environments. In this work, we perform, for the first time, a chemical modelling study of nitrogen fractionation that may be occurring in the gaseous component of external galaxies. In Section 2, we present the chemical model and network used for the ^{14}N and ^{15}N isotopic species; in Section 3, we present our results for the modelling of the nitrogen fractionation in gas at different H_2 densities and extinction, and affected by energetic phenomena [such as stellar heating, ultraviolet (UV) radiation, and cosmic rays]. In Section 4, we report our conclusions.

2 CHEMICAL MODELLING OF NITROGEN FRACTIONATION

The chemical modelling was carried out using the open source time-dependent gas–grain chemical code UCLCHEM.[1] The code is explained in detail in Holdship et al. (2017). Here we briefly summarize its main characteristics. UCLCHEM computes the evolution,

★ E-mail: sv@star.ucl.ac.uk

[1]https://uclchem.github.io/

as a function of time, of chemical abundances of the gas and on the ices starting from a diffuse and atomic gas. We ran UCLCHEM in two phases in a very similar manner as in Viti (2017) where theoretical abundances for extragalactic studies were derived. In Phase I, the gas is allowed to collapse and to reach a high density by means of a free-fall collapse. The temperature during this phase is kept constant at 10 K, and the cosmic ray ionization rate and radiation field are at their standard Galactic values of $\zeta_o = 5 \times 10^{-17}$ s^{-1} and 1 Draine, or 1.6×10^{-3} erg s^{-1} cm^{-2} (Draine 1978; Draine & Bertoldi 1996). During Phase I, atoms and molecules are allowed to freeze on to the dust grains and react with each other, forming icy mantles. In Phase II, we compute the chemical evolution of the gas after some energetic event has occurred [simulating either the presence of an active galactic nucleus (AGN) and/or a starburst].

The initial (solar) elemental abundances considered in our models were taken from Asplund et al. (2009). Our elemental isotopic nitrogen ratio is 440. UCLCHEM includes non-thermal desorption processes during the cold phase. Furthermore, UCLCHEM also includes thermal desorption processes as described in Viti et al. (2004), for this work we simply assume instantaneous evaporation for the second phase.

In both phases, the basic gas phase chemical network is based on the UMIST13 data base (McElroy et al. 2013) with updates from the KIDA data base (Wakelam et al. 2015). The surface reactions included in this model are assumed to be mainly hydrogenation reactions, allowing chemical saturation when possible. The network contains 2908 reactions and 239 chemical species. The number of reactions is reduced with respect to other networks reproducing the chemistry of molecular cloud/cores (e.g. Loison et al. 2019), but similar to other networks used to reproduce the chemistry of nearby galaxies (Viti et al. 2014).

For the ^{15}N network, we duplicated the ^{14}N network changing all ^{14}N by ^{15}N. We also added the ^{15}N exchange reactions used by Roueff et al. (2015, see their tables 1 and 2), with the only exception of those reactions involving ortho-H_2 and para-H_2 for which we only used the reaction rate from the ortho-H_2 species. This is partially justified because when we calculated the rate for the para and ortho species at 10 and 100 K, we systematically found that the ortho rate was orders of magnitude higher than the para ones. Nevertheless we note that, as some studies show (Furuya et al. 2015; Hily-Blant et al. 2018), in some environments para-H_2 may be dominant. We have therefore performed a further test where we use the rate for para-H_2 instead of the one for the ortho-H_2, essentially assuming in this way that all the molecular hydrogen is in the para form. The only two reactions affected by this exchange are

$$^{14}N^+ + H_2 \rightarrow NH^+ + H$$

$$^{15}N^+ + H_2 \rightarrow {}^{15}NH^+ + H$$

which essentially only affect ammonia and the nitrogen hydrides. We discuss this further in Section 3.4. For the ion–neutral reactions for which Roueff et al. (2015) do not give any reaction rate coefficient, we adopted the standard Langevin value of 10^{-9} cm^3 s^{-1} for the forward reaction, as done also by Hily-Blant et al. (2013). We have not included the reactions considered as improbable in table 1 of Roueff et al. (2015). Finally, we have also checked and updated (where needed) our network according to the reactions given in table 3 of Loison et al. (2019).

To test the network, we first ran a model with the same initial conditions as in Wirström & Charnley (2018). They assumed a static core with constant H_2 volume density of 10^6 cm^{-3}, constant gas temperature of 10 K, a cosmic ray ionization rate $\zeta = 3 \times 10^{-17}$ s^{-1}, and visual extinction $A_v = 10$ mag. In our test model, we have used these same input parameters, as well as the same initial elemental abundances of C, N, and O (taken from Savage & Sembach 1996). Usually, in our model carbon is, initially, totally in the atomic form (C or C^+), while Wirström & Charnley (2018) assume it is totally locked in CO. Therefore, we have adapted our model to also reproduce this initial condition. We find values of the HCN abundance with respect to H_2, and ^{14}N/^{15}N in HCN, very similar to those computed by Wirström & Charnley (2018): in our model, the HCN abundance rises up to $\sim 10^{-9}$ at $\sim 10^4$ yr, and then it drops by several orders of magnitude afterwards. We also find that ^{14}N/^{15}N for HCN/H^{15}N is about 400, as found by Wirström & Charnley (2018), and thus conclude that our updated model can reproduce the most recent dark cloud models including ^{15}N fractionation. We note that we have not considered the doubly substituted N_2, as done by Wirström & Charnley (2018), because we have assumed that this species is negligible for the chemistry of extragalactic environments at large scales. Our assumption is likely correct because we are able to reproduce the results of Wirström & Charnley (2018), which indicates that the reactions involving the doubly substituted N_2 are indeed negligible.

Following the approach of Wirström & Charnley (2018), we have replicated all reactions involving ^{14}N species, including those in which more than one product includes nitrogen. This could lead, at high densities and long times, to an artificial increase of the values of the isotopic ratios. Therefore, we recommend to consider these values at long evolutionary times with caution.

Our initial grid includes 288 models, spanning the following parameter space: gas final densities from 10^4 to 10^6 cm^{-3}, visual extinctions from 1 to 100 mag, temperatures of 50 and 100 K, radiation fields from 1 to 100 Draine, and cosmic ray ionization rates from 1 to 10^4 standard galactic cosmic ray ionization field, all selected to cover the ranges likely to be appropriate for external galaxies. The temperature, radiation field, and cosmic ray ionization rate vary only in Phase II. Our parameter space is motivated primarily by considering the parameters that affect most the line intensities of gas tracers in starburst and AGN-dominated galaxies, as predicted by radiative transfer models. We also note that our parameter ranges are consistent with previous studies of the chemistry in external galaxies (e.g. Bayet et al. 2009; Bayet, Awad & Viti 2010). Note that the cosmic ray ionization flux is also used to 'simulate' an enhancement in X-ray flux. As previously noted (Viti et al. 2014), this approximation has its limitations in that the X-ray flux will heat the gas more efficiently than cosmic rays. However, the chemistry arising from these two fluxes should be similar. In addition, we have ran a second grid of models, varying the parameter space as above, at a reduced metallicity of half solar, to mimic environments more similar to the Large Magellanic Cloud (LMC). While we do not aim at modelling any galaxy in particular, this parameter space ought to cover the range of possible differences between extragalactic environments, where nitrogen fractionation has been measured, and the Milky Way.

3 RESULTS

In this section, we describe our model predictions for ^{14}N/^{15}N by varying crucial physical and chemical parameters of the host galaxy, and discuss how they compare with observations. We have analysed the following chemical species: HCN, HNC (the only two species

Table 1. $^{14}N/^{15}N$ measured in external galaxies.

Galaxy	Type	$^{14}N/^{15}N$	Molecule	Reference
NGC 4945	Starburst	200–500	HCN	Henkel et al. (2018)
LMC	0.5 metal	111(±17)	HCN	Chin et al. (1999)
Arp 220	ULIRG	440 (+140, −82)	HCN, HNC	Wang et al. (2016)
NGC 1068	AGN + starburst	>419	HCN	Wang et al. (2014)
IC 694	Starburst	200–400(?)	HCN	Jiang, Wang & Gu (2011)
LMC	0.5 metal	91(±21)	HCN	Wang et al. (2009)
M82	Starburst	>100	HCN	Henkel et al. (1998)
Galactic Centre	Standard with high ζ	≥164	HNC	Adande & Ziurys (2012)

for which measurements have been obtained, see Table 1), CN, and N_2H^+. In the next section, we will start discussing the most abundant species, i.e. HCN and HNC, and its chemically related species CN.

3.1 Dependence of fractionation to variations in the physical parameters

A summary of the qualitative trends of the $^{14}N/^{15}N$ with time, as a function of the combination of the physical parameters, is given in Table 2. Although we run models for two representative average temperatures of 50 and 100 K, we find that varying the temperature does not lead to significant changes in the model predictions of the $^{14}N/^{15}N$ and hence we shall not discuss the sensitivity to temperature variations further.

Depending on the combinations of the various parameters, the largest variation with time that we find in $^{14}N/^{15}N$ for HCN, HNC, or CN is of an order of magnitude in a range from ∼10 to ∼1000. In Figs 1 and 2, we plot the predictions for $^{14}N/^{15}N$ against time showing the largest $^{14}N/^{15}N$ increase or decrease, respectively, while in Figs 3 and 4, we show the fractional abundances (with respect to the total number of hydrogen nuclei) of the main isotopologues for the same models. Fig. 1 shows that the largest increase is obtained either when $\zeta = 1000$ or when both ζ and χ are about 1000 times their standard values, and $A_V \geq 10$ mag. In all cases, the average density is low (10^4 cm^{-3}). This means that, at large giant molecular cloud scales (i.e. for $n_H \sim 10^4$ cm^{-3}), in galaxies with sources of energetic particles such as AGNs or ultraluminous infrared galaxies (ULIRGs) the fractionation should be suppressed with time. On the other hand, the highest drop in $^{14}N/^{15}N$ (Fig. 2) is found for two cases: if χ is low (1 Draine) but the gas density is high (10^6 cm^{-3}, top panel in Fig. 2), or when χ and A_V are high (1000 Draine and ≥10 mag, respectively) and the density is low (10^4 cm^{-3}, bottom panel in Fig. 2). A smaller but significant decrease is obtained also when ζ is high (1000) at high density (middle panel Fig. 2). We note that in the top and middle panels of Fig. 2, the ratios do not seem to reach a steady state but show a gradual decrease.

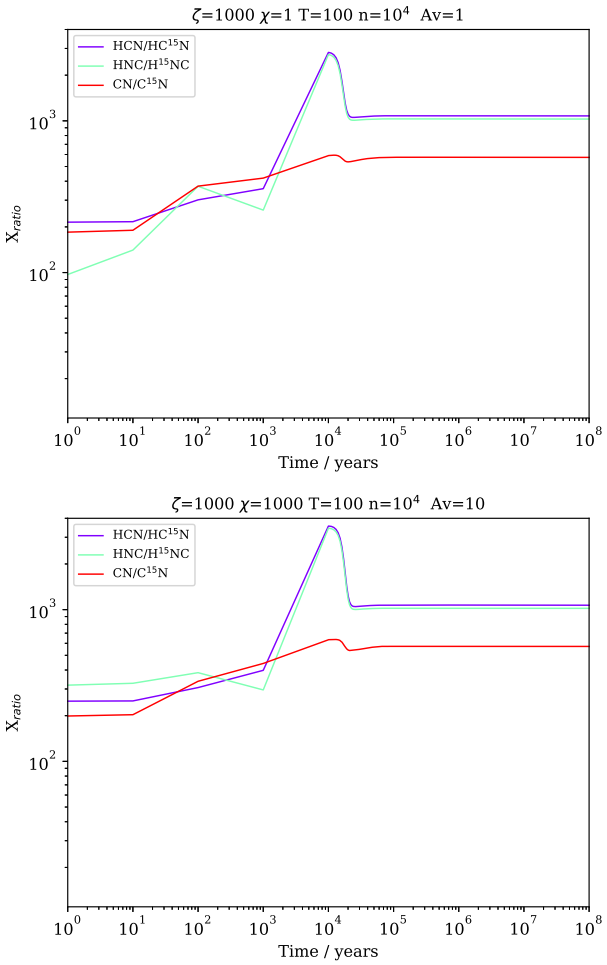

Figure 1. Plots showing the cases with significant $^{14}N/^{15}N$ increase, i.e. a fractionation decrease. In the title bar ζ is in units of ζ_o, χ in units of Draine, the temperature in units of K, the gas density in units of cm^{-3}, and the A_V is in magnitudes.

Table 2. Qualitative trends of fractionation as a function of different parameters.

Model	$A_V = 1$ mag	$A_V \geq 10$ mag
Standard	Constant, apart from a transient enrichment more pronounced for HCN	$^{14}N/^{15}N$ decrease of one order of magnitude after 10^6 yr especially at high density
High ζ	Decrease of fractionation at low densities with time, flat at high density	Decrease/increase of fractionation at low/high density (respectively) with time
High χ	Constant with time at both densities	Fractionation increase with time for both densities
High $\zeta + \chi$	Constant with time at both densities	Fractionation decrease/increase at low/high density, respectively

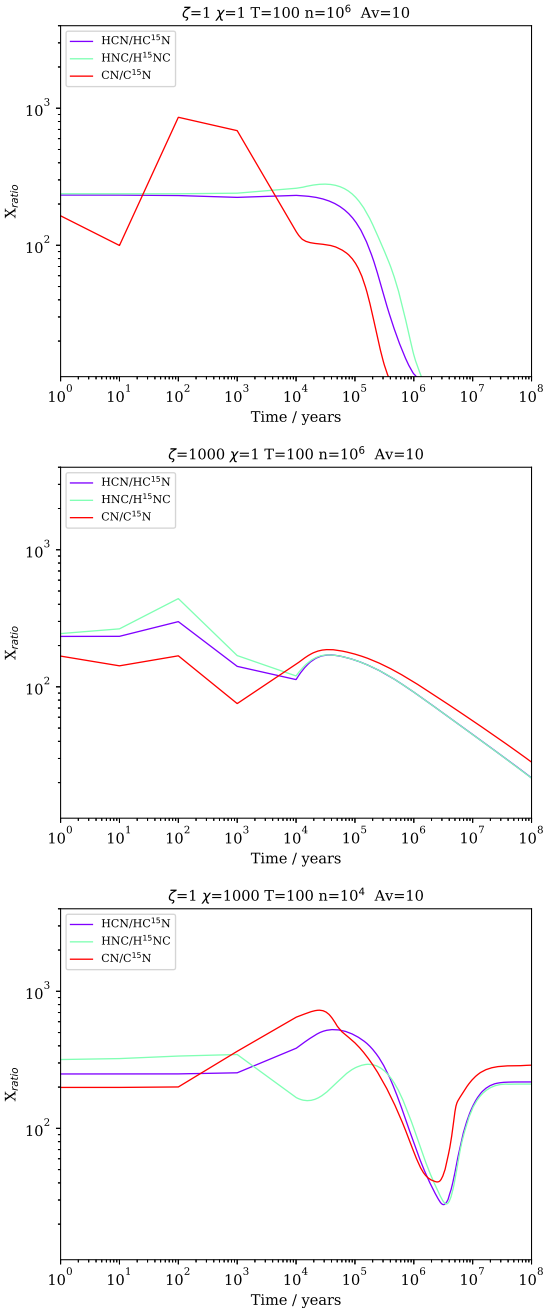

Figure 2. Plots showing the cases with significant $^{14}N/^{15}N$ decrease, i.e. a fractionation increase. Units as in Fig. 1.

We have quantified this decrease and found that in reality this is less than 5 per cent, and likely due to the precision of our calculations. The decrease of the ratios at long times appears large only because the logarithmic *Y*-scale tends to magnify the changes that occur at low ratios.

The above discussion describes our analysis of solar metallicity models. As mentioned in Section 2, we also ran models for metallicities half the solar one in order to reproduce the possible trend in a galaxy like the Small Magellanic Cloud (SMC), or other low-metallicity galaxies. In general, we do not find any significant difference in the trends. For some of the models we find slightly different absolute values of the $^{14}N/^{15}N$ but the range remains the same.

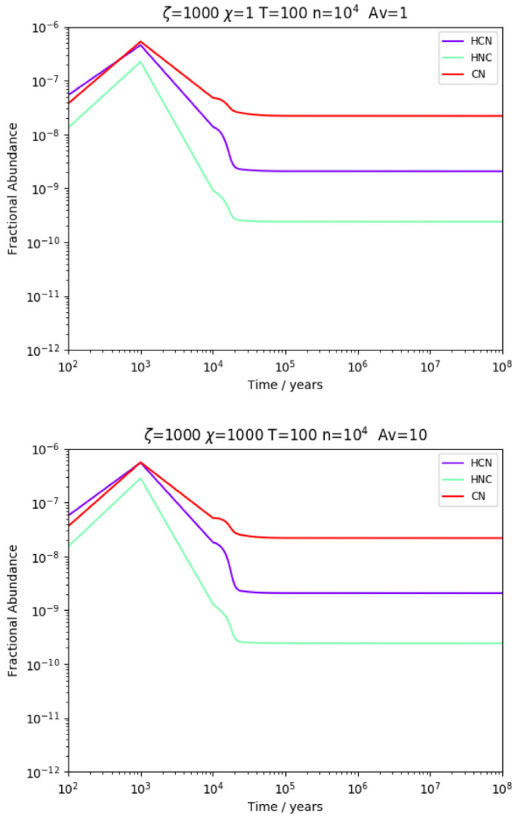

Figure 3. Plots showing the fractional abundances with respect to the total number of hydrogen nuclei of the main isotopologues of the models of Fig. 1.

3.2 Differences in fractionation among N-bearing molecules

One of the clearest results from our modelling is that HCN and HNC show little differences in their $^{14}N/^{15}N$ within a factor of 2. The fractionation of CN, on the other hand, shows more variability, especially with time for many models. In particular, for cosmic ray ionization rates $\geq$1000 the standard one, and densities $\leq 10^5$ cm^{-3}, the CN fractionation at late times is always higher than that of HNC and HNC by more than a factor of 2.

3.3 Comparison with observations

In Table 1, we list the observational values of $^{14}N/^{15}N$ for all external galaxies reported in the literature. As reference, in Table 3 we also list the average values (with the dispersions) of the $^{14}N/^{15}N$ obtained in massive star-forming clumps and diffuse clouds in the Milky Way. The Milky Way can be considered as a template for spiral galaxies, hence these clumps represent a proxy of the densest portions in spirals. We do not include in the table low-mass star-forming cores.

Unfortunately, the only two species detected in the ^{15}N isotope in external galaxies are HCN and (in fewer places) HNC. Hence, we focus the comparison with our models on HCN. Our criterion for choosing the models that best reproduce the observations is that the ratio has to be matched by 10^5 yr and be maintained up to a million year. For the galaxies where we only have a lower limit for this ratio, we have imposed an arbitrary upper limit of 1000.

We note that in general many models match the observed value of fractionation, indicating that the observed ratio is achievable under a large range of physical and chemical parameters. More

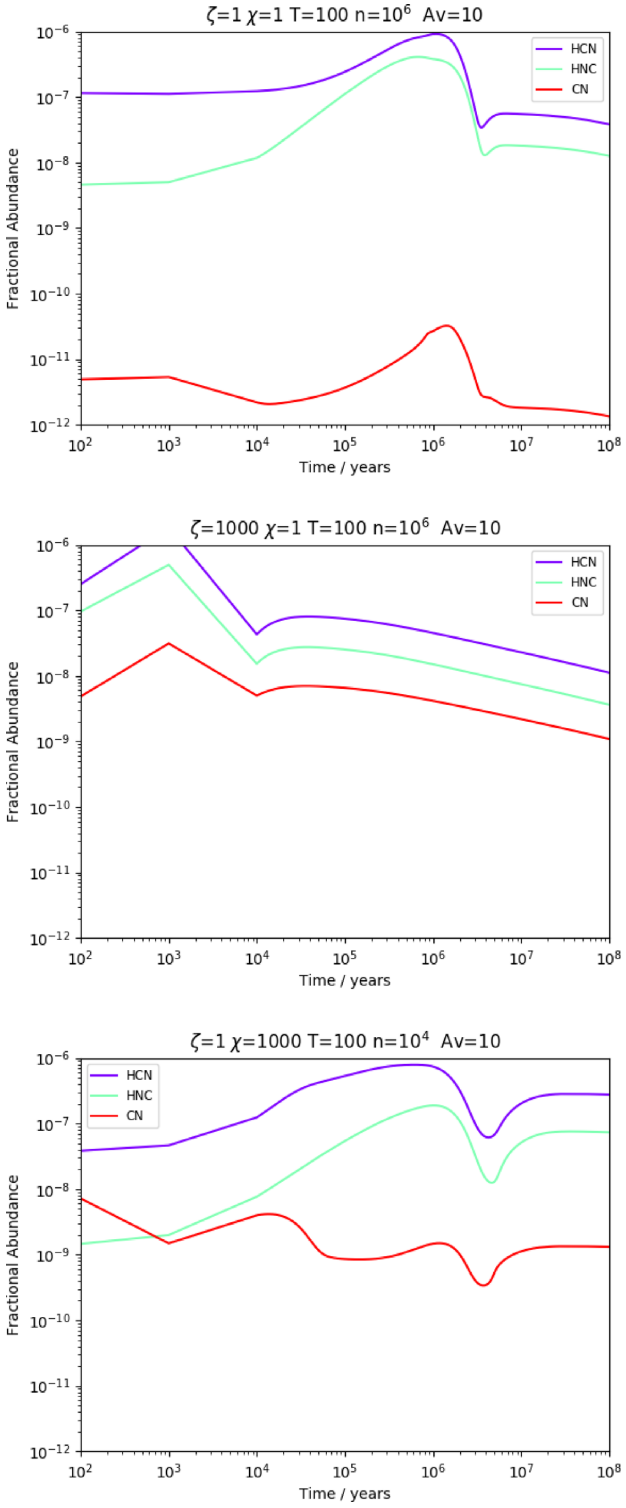

Figure 4. Plots showing the fractional abundances of the main isotopologues with respect to the total number of hydrogen nuclei of the models of Fig. 2.

specifically, for both NGC 4945 and Arp 220, the range of observed values is achieved by models of gas at low visual extinction for gas densities up to 10^5 cm^{-3} and cosmic ray ionization rate up to 100 the standard value. However, for NGC 4945 there are also some models at high densities (10^6 cm^{-3}) at all cosmic ray ionization rates that can match the observed ratio at low and high visual extinctions. For Arp 220, densities of 10^6 cm^{-3} can only match observations for the highest cosmic ray ionization rates and highest radiation fields at low visual extinctions. This may in fact be consistent with the high star formation rates found in the nuclear region of this galaxy. We note that only for these high densities the radiation field has an impact on the fractionation ratio. IC 694 has similar ranges of fractionation to NGC 4945 but with a lower upper limit and this indeed reduces the best matches among the models: here only densities $\geq 10^5$ cm^{-3} fit the observed fractionation and, for 10^5 cm^{-3}, only at visual extinctions of 1 mag for cosmic ray ionization rates and radiation fields of up to 100 and 10 the standard value, respectively. For higher densities, higher values of radiation, cosmic rays, and, in some cases, visual extinction also match the ratio. For the galaxies where we only have lower limits, even imposing an upper limit of 1000, lead to too many models matching the ratio to discuss them here. For the LMC, on the other hand, we are able to constrain the physical parameters much better, as there are only very few models that match the observations: a model with a gas density of 10^5 cm^{-3} with a standard galactic cosmic ray ionization rate and an A_V of >10 mag, or models with a density of 10^6 cm^{-3}, $A_V \geq 10$ mag, and $\zeta > 100$ the standard value. In fact, the measured extinction in the LMC is significantly lower than the average found in the Milky Way (Dobashi et al. 2008), so the first case may be favoured. The radiation field is not constrained.

Together with the results from Sections 3.1 and 3.2, we can conclude that the main cause of enrichment in ^{15}N is high densities, but it can be aided by high fluxes of cosmic rays and, to a lesser extent, an intense radiation field.

3.4 Fractionation predictions for N_2H^+ and NH_3 in external galaxies

Not many nitrogen-bearing species have been observed to be abundant in external galaxies. Besides HCN, HNC, and CN, discussed already in previous sections, the most common nitrogen-bearing species detected in nearby galaxies are HNCO, HC_3N, CH_3CN, and N_2H^+. While our network does include all the ^{14}N isotopologues of these species, a fractionation chemistry for the first three of these species is not available, and hence we concentrate on the predicted fractionation of N_2H^+, an important tracer of cold and dense gas.

Aladro et al. (2015) detected N_2H^+ in four galaxies: M83, NGC 253, M82, and M51, and found a column density of 6.5×10^{12}, 4×10^{13}, 1×10^{13}, and 4×10^{12} cm^{-2}, respectively. Grouping M83 with M51 and M82 with NGC 253 (due to their similar values of observed N_2H^+) we find that for the first two galaxies this translates into a N_2H^+ fractional abundance ranging between 2.5 and 4×10^{-10} if the visual extinction is 10 mag, and 2.5 and 4×10^{-11} if the visual extinction is 100 mag. For the other two galaxies, we get an abundance of $\sim 6.2 \times 10^{-10}$–2.5×10^{-9} for 10 mag and $\sim 6 \times 10^{-11}$–2.5×10^{-10} for 100 mag. In order to predict the expected fractionation of N_2H^+ in these galaxies we restrict our grid of models to those that match these abundances.

M83 and M51. We find that if the visual extinction traced by N_2H^+ is close to 10 mag, then two models can reproduce the range of abundances but both only for *a short* period of time, in some cases as brief as 1000 yr: a model with a cosmic ray ionization rate higher than the galactic standard one by a factor of 1000, a gas temperature of 50 K, and a gas density of 10^4 cm^{-3}, and another model with a cosmic ray ionization rate higher than the galactic standard one by a factor of 10 000, a gas temperature of 100 K, and a gas density of 10^5 cm^{-3}. Clearly, N_2H^+ is tracing dense gas but it is interesting to note that

Table 3. $^{14}N/^{15}N$ measured in the Milky Way in dense and diffuse clouds from different molecules.

Reference	$^{14}N/^{15}N$			
	HCN	HNC	CN	N_2H^+
Adande & Ziurys (2012)		∼130–400	∼120–380	
Fontani et al. (2015)			190–450	180–1300
Ritchey, Federman & Lambert (2015)			274 ± 18	
Colzi et al. (2018b)	115–1305	185–780		
Zeng et al. (2017)	70–763	161–541		

only high levels of cosmic ray ionization rate can maintain its abundance if the temperature of the gas is >10 K. If the gas has a visual extinction of 100 mag, then the only models that achieve to maintain a high abundance of N_2H^+ have a cosmic ray ionization rate of 100 times that of the galactic one, a temperature of 50 or 100 K and a gas density of 10^4 cm^{-3}. In this case, however, N_2H^+ is not destroyed before 10 000 yr. We note that both M51 and M83 are spiral galaxies, with M83 being a young starburst and M51 having recently interacted with a nearby galaxy triggering star formation. Hence both are likely to have an enhanced cosmic ray ionization rate.

M82 and NGC 253. At 10 mag the only model that reproduces the observed abundance of N_2H^+ is one with a high cosmic ray ionization rate (1000 ζ_o), a temperature of 100 K, and a gas density of 10^4 cm^{-3}, while if the gas is at a visual extinction of 100 mag, then the same model but with a factor of 10 less cosmic ray ionization rate can reproduce the observed abundance of N_2H^+. We recall that the derived abundances from the observations are different at different extinctions that is why for this comparison models at different visual extinctions do give different matches. We note that these two galaxies are the prototypical chemically rich starburst galaxies and, again, as for the other two galaxies, a higher than standard cosmic ray ionization rate is expected. We also note that while the abundance of N_2H^+ is not sensitive to changes in the radiation field, for all our best-fitting models the latter cannot exceed ∼100–1000 Draine.

These results indicate that either the observed N_2H^+ is tracing in fact colder gas than we modelled, or that it is indeed tracing gas close to a source of high cosmic ray flux that maintains its abundance for longer. In order to exclude the former hypothesis we ran a test model whereby we maintained in Phase 2 all the parameters as in Phase 1 (including the temperature of the gas at 10 K) and ran the model for 10^7 yr. We find that, regardless of the gas density, we cannot obtain an N_2H^+ abundance much higher than 10^{-11} (which is below the observational value for most observations) for times less than 1 Myr (see Fig. 5). Hence we conclude that the high abundance of N_2H^+ is indeed a consequence of the cosmic ray ionization rate but that it is indeed transient implying that the gas traced by N_2H^+ and observed by Aladro et al. (2015) is young or most likely replenished periodically. Our predictions also imply that high N_2H^+ abundances are preferentially seen towards young galaxies, and thus N_2H^+ could be potentially an evolutionary indicator, although this conclusion has to be taken with caution given the large number of parameters that should produce the predicted high N_2H^+ abundance.

What do these best-matching models predict in terms of fractionation? Surprisingly the ratio of N_2H^+ to either of its fractionated counterparts is *always* at least 10^4 implying an extremely low fractionation. Assuming that our chemical network for the fractionation of N_2H^+ is complete, it is therefore unlikely we would be able to detect $^{15}NNH^+$ or $N^{15}NH^+$ in a reasonable amount of integration time even with the current, most powerful facilities.

Finally, it is worth briefly discussing our predictions for NH_3 fractionation. Ammonia was detected in NGC 253 (Ott et al. 2005), yielding a temperature ≤17–85 K. We plot in Fig. 6 the ammonia isotopic ratio expected in the best-fitting model for NGC 253. As we can see from the figure, for gas older than 10 000 yr the predicted fractionation is far too low to be detectable. As mentioned in Section 2, omitting the reactions with para-H_2 may have consequences for the abundance of hydrogen nitrides. We therefore compared the NH_3 gas fractional abundance between our model and the one performed assuming all the molecular hydrogen in the para form, as described in Section 2, but found that while

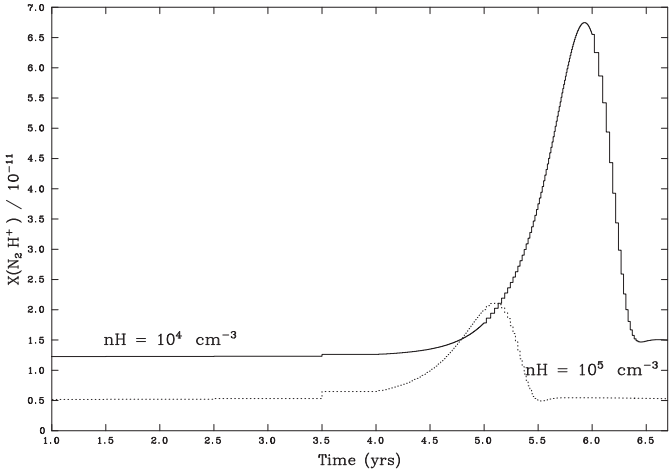

Figure 5. Fractional abundance of N_2H^+ as a function of time for Phase 2 of two models varying in gas densities, at a constant temperature of 10 K (see text).

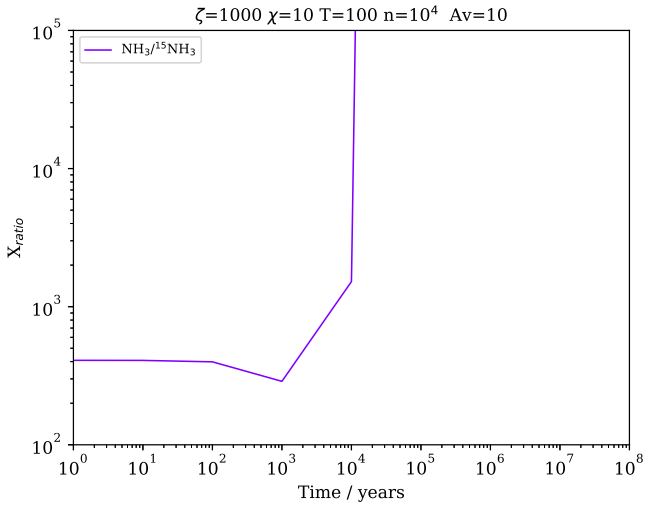

Figure 6. NH_3 fractionation for one of the best-fitting model for NGC 253 as derived from the N_2H^+ observations.

they differ by a factor of 2 at the end of the cold phase, they are essentially the same in Phase 2. This is because once the gas is heated to ∼100 K, the ammonia formed on the ices via hydrogenation is released back to the gas phase and any difference in its abundance between the two models disappears.

4 CONCLUSIONS

We have used a time-dependent gas–grain chemical model to determine the nitrogen fractionation of dense gas under a range of physical parameters representing galaxies with intense far-UV or cosmic ray sources. We determine the sensitivity of the fractionation to the local physical conditions, as well as the fractionation differences among the observable nitrogen-bearing species; we qualitatively test our models by comparing our findings with the few observations of HCN available and we then make some predictions related to the fractionation for an important nitrogen-bearing species, N_2H^+. We summarize our findings below.

(i) In general we find that in most models the $^{14}N/^{15}N$ for HCN, HNC, or CN never varies by more than an order of magnitude with time, and remains in a range from ∼100 to ∼1000.

(ii) An increase in fractionation can occur at low radiation fields and high densities and vice versa, as well as when both the cosmic ray ionization rate and the gas density are high.

(iii) A decrease in fractionation is obtained at low densities, high visual extinction, and high fluxes of either radiation fields or cosmic rays.

(iv) HCN and HNC show little differences in their $^{14}N/^{15}N$ within a factor of 2. On the other hand the $^{14}N/^{15}N$ for CN can be different from that of the other two species at late times for densities $\leq 10^5$ cm^{-3} and cosmic ray ionization rates to $\geq$1000 the standard one.

(v) Our models succeed in reproducing the observed $^{14}N/^{15}N$ in external galaxies but due to the large ranges observed we are unable to fully constrain the physical parameters of each galaxy with the exception of the LMC whose nitrogen fractionation implies a gas density of 10^5 cm^{-3} with galactic cosmic ray ionization rate and an A_V of 100 mag, or a density of 10^6 cm^{-3}, $A_V > 10$ mag, and $\zeta > 100$.

(vi) Finally, we predict that even with the most sensitive instruments to date it is unlikely that we would be able to detect $^{15}NNH^+$ or $N^{15}NH^+$ in external galaxies as their fractionation is more than one order of magnitude lower than that for HCN, HNC, or CN.

ACKNOWLEDGEMENTS

SV and JH acknowledge STFC grant ST/M001334/1. IJ-S acknowledges partial support by the MINECO and FEDER funding under grants ESP2015-65597-C4-1 and ESP2017-86582-C4-1-R. We are grateful to E. Wirström and J.-C. Loison for providing us useful clarifications about their models, to C. Henkel for critical reading of the manuscript, and to the anonymous referee for constructive comments that improved the paper.

REFERENCES

Adande G. R., Ziurys L. M., 2012, ApJ, 744, 194
Aladro R. et al., 2015, A&A, 579, A101
Asplund M., Grevesse N., Sauval A. J., Scott P., 2009, ARA&A, 47, 481
Bayet E., Awad Z., Viti S., 2010, ApJ, 725, 214
Bayet E., Viti S., Williams D. A., Rawlings J. M. C., Bell T., 2009, ApJ, 696, 1466
Bizzocchi L., Caselli P., Leonardo E., Dore L., 2013, A&A, 555, A109
Chin Y.-N., Henkel C., Langer N., Mauersberger R., 1999, ApJ, 512, L143
Clayton D. D., 2003, Ap&SS, 285, 353
Colzi L., Fontani F., Caselli P., Ceccarelli C., Hily-Blant P., Bizzocchi L., 2018a, A&A, 609, A129
Colzi L., Fontani F., Rivilla V. M., Sánchez-Monge A., Testi L., Beltrán M. T., Caselli P., 2018b, MNRAS, 478, 3693
De Simone M. et al., 2018, MNRAS, 476, 1982
Dobashi K., Bernard J.-P., Hughes A., Paradis D., Reach W. T., Kawamura A., 2008, A&A, 484, 205
Draine B. T., 1978, ApJS, 36, 595
Draine B. T., Bertoldi F., 1996, ApJ, 468, 269
Fontani F., Caselli P., Bizzocchi L., Ceccarelli C., Hily-Blant P., 2015, ApJ, 808, L46
Fouchet T., Irwin P. G. J., Parrish P., Calcutt S. B., Taylor F. W., Nixon C. A., Owen T., 2004, Icarus, 172, 50
Furuya K., Aikawa Y., Hincelin U., Hassel G. E., Bergin E. A., Vasyunin A. I., Herbst E., 2015, A&A, 584, A124
Füri E., Marty B., 2015, Nat. Geosci., 8, 515
Guzmán V. V., Öberg K. I., Huang J., Loomis R., Qi C., 2017, ApJ, 836, 30
Henkel C., Chin Y.-N., Mauersberger R., Whiteoak J. B., 1998, A&A, 329, 443
Henkel C. et al., 2018, A&A, 615, A155
Hily-Blant P., Bonal L., Faure A., Quirico E., 2013, Icarus, 223, 582
Hily-Blant P., Faure A., Rist C., Pineau des Forêts G., Flower D. R., 2018, MNRAS, 477, 4454
Holdship J., Viti S., Jiménez-Serra I., Makrymallis A., Priestley F., 2017, AJ, 154, 38
Izzard R. G., Tout C. A., Karakas A. I., Pols O. R., 2004, MNRAS, 350, 407
Jiang X., Wang J., Gu Q., 2011, MNRAS, 418, 1753
Kahane C., Jaber Al-Edhari A., Ceccarelli C., López-Sepulcre A., Fontani F., Kama M., 2018, ApJ, 852, 130
Loison J.-C., Wakelam V., Gratier P., Hickson K. M., 2019, MNRAS, 484, 2747
Marty B., Kelley S., Turner G., 2010, Geochim. Cosmochim. Acta, 74, 6636
Matteucci F., 1986, MNRAS, 221, 911
McElroy D., Walsh C., Markwick A. J., Cordiner M. A., Smith K., Millar T. J., 2013, A&A, 550, A36
Mumma M. J., Charnley S. B., 2011, ARA&A, 49, 471
Ott J., Weiss A., Henkel C., Walter F., 2005, ApJ, 629, 767
Prantzos N., 2011, in 11th Symposium on Nuclei in the Cosmos, Topics on Galactic Chemical Evolution, preprint (arXiv:1101.2108)

Redaelli E., Bizzocchi L., Caselli P., Harju J., Chacón-Tanarro A., Leonardo E., Dore L., 2018, A&A, 617, A7
Ritchey A. M., Federman S. R., Lambert D. L., 2015, ApJ, 804, L3
Romano D., Matteucci F., 2003, MNRAS, 342, 185
Romano D., Matteucci F., Zhang Z.-Y., Papadopoulos P. P., Ivison R. J., 2017, MNRAS, 470, 401
Roueff E., Loison J. C., Hickson K. M., 2015, A&A, 576, A99
Savage B. D., Sembach K. R., 1996, ARA&A, 34, 279
Schmitt J. H. M. M., Ness J.-U., 2002, A&A, 388, L13
Viti S., 2017, A&A, 607, A118
Viti S., Collings M. P., Dever J. W., McCoustra M. R. S., Williams D. A., 2004, MNRAS, 354, 1141
Viti S. et al., 2014, A&A, 570, A28
Wakelam V. et al., 2015, ApJS, 217, 20
Wang J., Zhang Z.-Y., Qiu J., Shi Y., Zhang J., Fang M., 2014, ApJ, 796, 57
Wang J., Zhang Z.-Y., Zhang J., Shi Y., Fang M., 2016, MNRAS, 455, 3986
Wang M., Chin Y.-N., Henkel C., Whiteoak J. B., Cunningham M., 2009, ApJ, 690, 580
Wirström E. S., Charnley S. B., 2018, MNRAS, 474, 3720
Zeng S. et al., 2017, A&A, 603, A22

This paper has been typeset from a TEX/LATEX file prepared by the author.